

Seasonality in the relationship between El Nino and Indian Ocean dipole

Mathew Roxy · Silvio Gualdi ·
Hae-Kyung Lee Drbohlav · Antonio Navarra

Received: 7 December 2009 / Accepted: 25 June 2010 / Published online: 6 July 2010
© Springer-Verlag 2010

Abstract The seasonal change in the relationship between El Nino and Indian Ocean dipole (IOD) is examined using the European Centre for Medium-Range Weather Forecasts (ECMWF) Re-Analysis (ERA-40), and the twentieth century simulations (20c3m) from the Geophysical Fluid Dynamics Laboratory Coupled Model, version 2.1. It is found that, both in ERA-40 and the model simulations, the correlation between El Nino (Nino3 index) and the eastern part of the IOD ($90\text{--}110^{\circ}\text{E}$; 10°S -equator) is predominantly positive from January to June, and then changes to negative from July to December. Correlation maps of atmospheric and oceanic variables with respect to the Nino3 index are constructed for each season in order to examine the spatial structure of their seasonal response to El Nino. The occurrence of El Nino conditions during January to March induces low-level anti-cyclonic circulation anomalies over the southeastern Indian Ocean, which counteracts the climatological cyclonic circulation in that region. As a result, evaporation decreases and the southeastern Indian Ocean warms up as the El Nino proceeds,

and weaken the development of a positive phase of an IOD. This warming of the southeastern Indian Ocean associated with the El Nino does not exist past June because the climatological winds there develop into the monsoon-type flow, enhancing the anomalous circulation over the region. Furthermore, the development of El Nino from July to September induces upwelling in the southeastern Indian Ocean, thereby contributing to further cooling of the region during the summer season. This results in the enhancement of a positive phase of an IOD. Once the climatological circulation shifts from the boreal summer to winter mode, the negative correlation between El Nino and SST of the southeastern Indian Ocean changes back to a positive one.

Keywords Indian Ocean dipole · El Nino · ENSO

1 Introduction

One of the distinct spatial structures of the Indian Ocean on interannual timescales is the zonal gradient of sea surface temperature (SST) from the tropical western Indian Ocean ($50\text{--}70^{\circ}\text{E}$, $10^{\circ}\text{S}\text{--}10^{\circ}\text{N}$) to the tropical southeastern Indian Ocean ($90\text{--}110^{\circ}\text{E}$, 10°S -equator). The difference in SST anomalies between these two regions is defined as the Indian Ocean dipole (IOD; Saji et al. 1999; Webster et al. 1999), and it influences the weather of the surrounding and remote areas of the Indian Ocean region (Black et al. 2003; Saji and Yamagata 2003a; Terray et al. 2003; Ashok et al. 2004; Behera et al. 2005). A positive IOD is characterized by strong positive SST anomalies in the tropical western Indian Ocean and the negative SST anomalies in the tropical southeastern Indian Ocean.

M. Roxy · S. Gualdi · A. Navarra
Centro-Euro-Mediterraneo per i Cambiamenti Climatici,
Bologna, Italy

S. Gualdi · A. Navarra
Istituto Nazionale di Geofisica e Vulcanologia, Bologna, Italy

H.-K. L. Drbohlav
International Pacific Research Center,
University of Hawaii at Manoa, Honolulu, HI, USA

M. Roxy (✉)
Centre for Climate Change Research,
Indian Institute of Tropical Meteorology,
Pune 411008, India
e-mail: roxy@tropmet.res.in

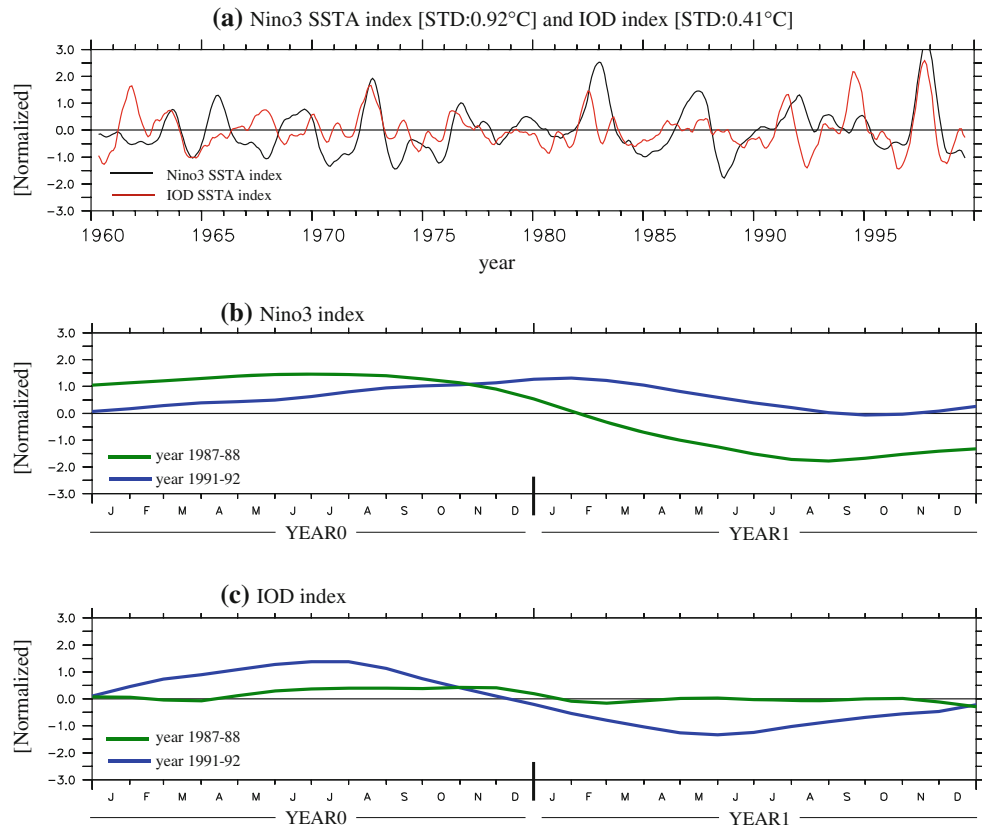
Often, the formation of the IOD coincides with the development of El Nino in the Pacific. As the mature phase of El Nino approaches, easterlies form over the tropical western Indian Ocean, and southeasterlies over the southeastern Indian Ocean strengthen (Drbohlav et al. 2007). Southeasterlies over the southeastern part of the basin reduce the oceanic mixed layer temperature by increasing the latent heat flux, cold meridional advection, and entrainment. Meanwhile, easterlies over the northwestern Indian Ocean increase the mixed layer temperature by inducing an anomalous westward ocean current that advects the warm seasonal mean mixed layer from the central to western Indian Ocean, and by reducing the upwelling along the Somali coast (Drbohlav et al. 2007).

Although this concurrence of El Nino and IOD has been studied extensively in the last several years (e.g. Annamalai et al. 2003; Gualdi et al. 2003; Lau and Nath 2003; Li et al. 2003; Loschnigg et al. 2003; Shinoda et al. 2004a; Cai et al. 2005), there are other observations that make it difficult to establish a direct correlation between El Nino and IOD. For example, the linear relationship between El Nino and IOD is not supported by statistical analysis (Saji et al. 1999; Yamagata et al. 2002; Saji and Yamagata 2003b). The correlation coefficient ($r = 0.34$) between IOD index and Nino3 SST anomaly time series is statistically insignificant (Saji et al. 1999; Webster et al. 1999;

Yuan and Li 2008). This is confirmed by coupled general circulation model simulations that can simulate IOD without El Nino (Iizuka et al. 2000; Fischer et al. 2005). However, the correlations increase, and become significant if calculated on monthly or seasonally stratified values of the indices, for example between mean September–November values of the IOD index and Nino3 SST (Allan et al. 2001). The above studies based on observations and model simulations reveals that the El Nino–IOD connection has a complex nature, rather than a simple linear relationship. Thus, in order to evaluate the relationship between El Nino and IOD, it is important to understand (1) why certain IODs develop independently from El Nino and (2) why the IOD is absent during certain El Ninos.

The existence of IOD in the absence of El Nino has been described in a number of studies in which observed and modeled IODs during non-El Nino years are analyzed (Annamalai et al. 2003; Shinoda et al. 2004b; Fischer et al. 2005; Drbohlav et al. 2007; Song et al. 2007a). The general consensus of these analyses is that IOD in non-El Nino years is formed due to “El Nino-like wind conditions”, especially in the eastern part of the Indian Ocean. In other words, as long as southeasterlies prevail in the southeastern Indian Ocean, the positive feedback through surface evaporation, ocean mixing and upwelling can induce the cooling of the eastern Indian Ocean. This cooling of the

Fig. 1 (a) Nino3 and IOD SST anomaly indices, normalized by their standard deviation, for the period 1960–1999, in the ERA-40 reanalysis data. Normalized (b) Nino3 and (c) IOD SSTA indices for the years 1987–1988 and 1991–1992. The climatology from 1960 to 1999 is used to calculate the anomalous monthly SST. Then, 8-month running mean is applied to these anomalies in order to highlight the interannual variability



eastern Indian Ocean contributes to establish the zonal temperature gradient that satisfies the definition of IOD.

The second question of “why the IOD is absent or trivial during certain El Niños” remains to be discussed. In particular, why do we see years with a relatively strong El Niño signal and no evidence of IOD whereas other years with a weak El Niño exhibits relatively strong IOD? The present study emphasizes its main objectives based on the queries cited above, and intends to provide possible mechanisms detailing the relationship.

The work is organized as follows: in Sect. 2, the data and the model utilized in the study are described. In Sect. 3, the seasonal variation of Nino3 and IOD in the data and the model is examined. The spatial structure of the seasonality is shown in Sect. 4, followed by a summary and discussion in Sect. 5.

2 Data and model

For the data, we use the ERA-40 reanalysis of the European Center for Medium-Range Weather Forecasts (ECMWF). Understanding of the seasonality in the relationship between El Niño and IOD, obtained from ERA-40 reanalysis, is limited due to the small sample size of 40 years. In order to increase the sample size of the analysis, we have examined a series of simulations produced for the Intergovernmental Panel on Climate Change (IPCC) Fourth Assessment Report (AR4). More specifically, we choose the twentieth century simulations by the 2.1 version of the coupled atmospheric-ocean general circulation model at Geophysical Fluid Dynamics Laboratory (GFDL) (GFDL_CM_2.1; hereafter simply CM2.1 for the sake of brevity). The 140 years of monthly data are obtained from

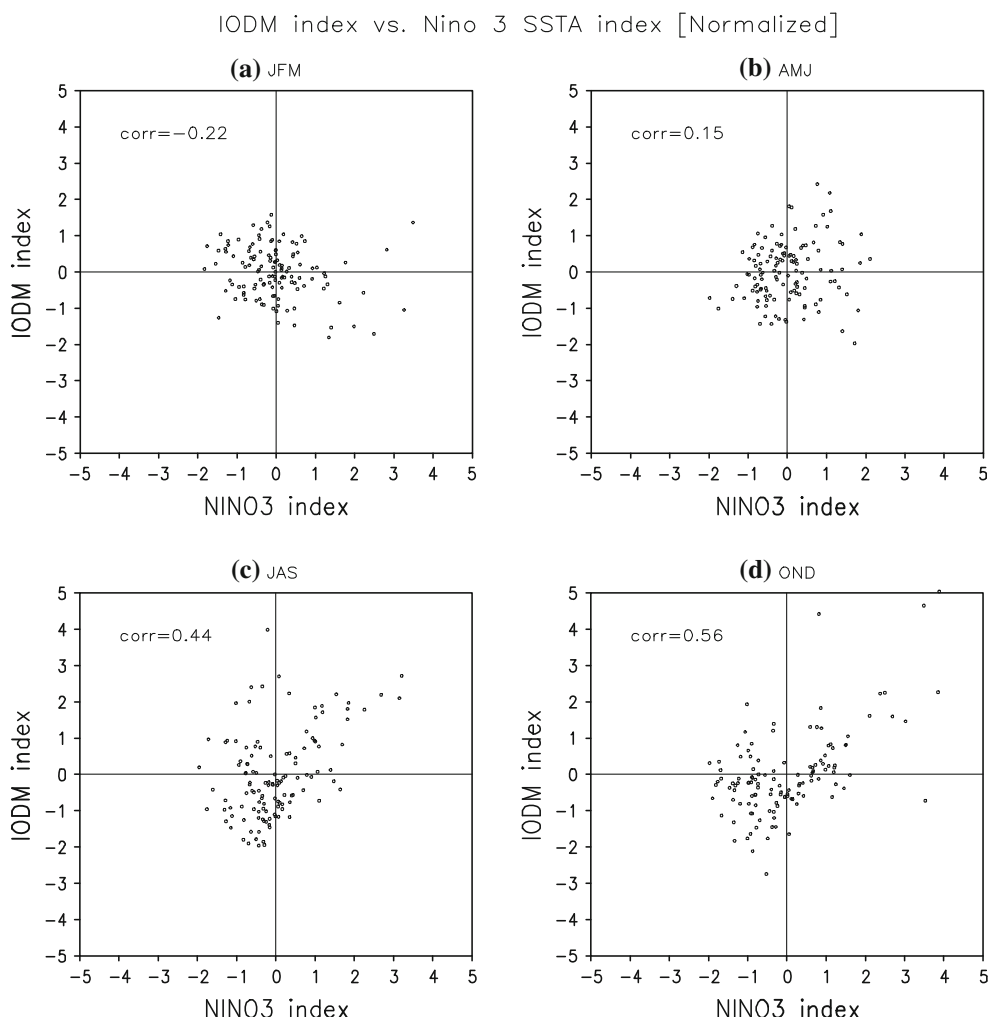


Fig. 2 Scatter plot and correlation between Nino3 SSTA and IOD indices, normalized by their standard deviation, for **a** JFM, **b** AMJ, **c** JAS, and **d** OND. Nino3 SSTA and IOD indices are calculated using ERA-40 reanalysis monthly data from 1959 to 1999

the five sets of twentieth century simulation of CM2.1 (hereafter addressed as 20c3m).

The atmospheric model of CM2.1 has a horizontal resolution of 2° in latitude by 2.5° in longitude with 24 levels in the vertical. The ocean model is based on the Modular Ocean (MOM4; Griffies et al. 2003) and has a 1° resolution. The meridional resolution of MOM4 varies from a minimum of $1/3^{\circ}$ between 30°S and 30°N to a maximum of 1° at the northern boundary. The 50 vertical levels are unevenly spaced with the first 22 levels confined to upper 220 m. The further information on the GFDL_CM_2.1 coupled model and its physical packages can be found in Delworth et al. (2006) and Anderson et al. (2004).

Ability of the CM2.1 in representing the interannual variability of Pacific and the Indian Oceans has been previously examined by Wittenberg et al. (2006) and Song et al. (2007a), respectively. In general, the model is reasonably realistic in reproducing many of the climatological features, and general characteristics of the interannual variability of El Nino and the IOD. Over the Pacific, the

model has a robust El Nino Southern Oscillation (ENSO) with irregular period between 2 and 5 years, a distribution of SST anomalies that is skewed towards warm events, and a realistic evolution of subsurface temperature anomalies. Also, over the Indian Ocean, the model reasonably simulates both the monsoon wind reversal and the seasonal cycle of SST and surface ocean currents (Song et al. 2007a). The model is also successful in simulating the ENSO-induced interannual SST variability in the Indian Ocean and the IOD events. This makes the CM2.1 a suitable candidate in examining the El Nino–IOD relationship.

In the 20c3m simulation the time varying forcing agents are inserted from 1860 to 2000, and five parallel model runs are provided using this design. Those forcing agents are atmospheric CO_2 , CH_4 , N_2O , halons, tropospheric and stratospheric O_3 , anthropogenic tropospheric sulfates, black and organic carbon, volcanic aerosols, solar irradiance, and the distribution of land cover types. For the purpose of our study we used monthly data from 1861 to 2000 of five parallel runs. Thus, the total sample size of

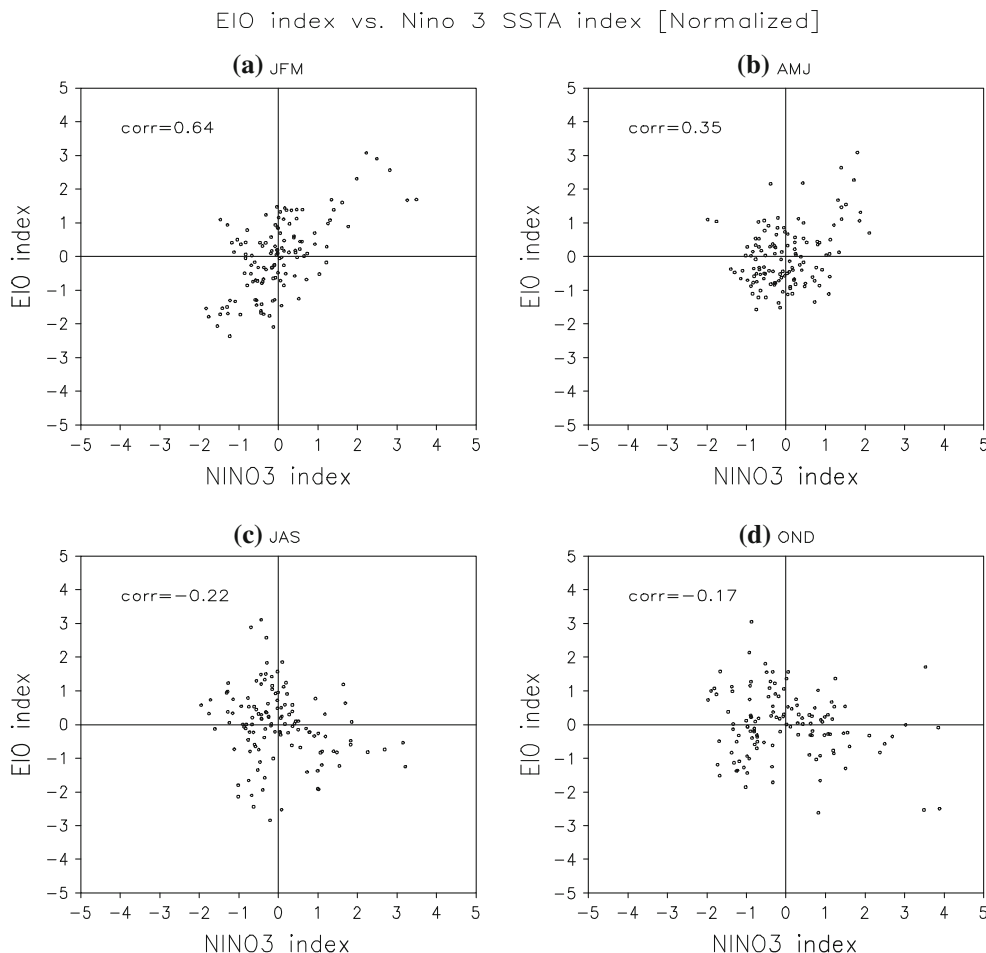


Fig. 3 Scatter plot and correlation between Nino3 SSTA index and the eastern component of IOD index (EIO; 90–110E, 10S-Equator), normalized by their standard deviation, for **a** JFM, **b** AMJ, **c** JAS, and

d OND. Nino3 SSTA and EIO indices are calculated using ERA-40 reanalysis monthly data from 1959 to 1999

each season is 700 years ($140 \text{ years} \times 5 \text{ runs} = 700 \text{ years}$). From these 700 years of seasonal mean data, the scatter plot between El Nino and IOD are constructed (Sect. 3). In addition, the temporal correlation between Nino3 and atmospheric (ocean) variables is calculated at each grid point in an attempt to examine the varying spatial structure of SST, wind stress, sea level pressure, and oceanic vertical motion associated with the El Nino in different seasons (Sect. 4).

3 Seasonal variation in the relationship between Nino3 and IOD

Figure 1 shows the evolution of the Nino3 and IOD indices for the years 1987–1988 and for the years 1991–1992, from the ERA-40 reanalysis. For the sake of clarity, years 1987 and 1991 will be indicated as YEAR0 and years 1988 and 1992 as YEAR1 in the discussion of the respective events.

Year 1987 is characterized by strong El Nino anomalous conditions; however the IOD signal is marginal. In other words, in 1987 we do not observe any IOD even if in this year the El Nino anomalies in the Pacific are larger than in other years when relatively weak El Nino events are accompanied by IODs (e.g. 1991). It suggests that the strength of El Nino alone may not be sufficient to predict the formation of IOD. Thus, in this study we investigate the other aspects of El Nino that could affect the formation of IOD. More specifically, how the phase locking between annual cycle and El Nino forcing influences the formation of IOD is examined. A Nino3 index (Fig. 1a) is used to identify the interannual variability of the El Nino. The Nino3 index is defined as an average of the SST in the eastern tropical pacific (Nino3 region; 150°W – 90°W , 5°S – 5°N). As shown in Fig. 1b, the Nino3 index in 1987 is already above one standard deviation in January, whereas the Nino3 index in 1991 barely reaches a half standard deviation till April. How does the positive forcing of

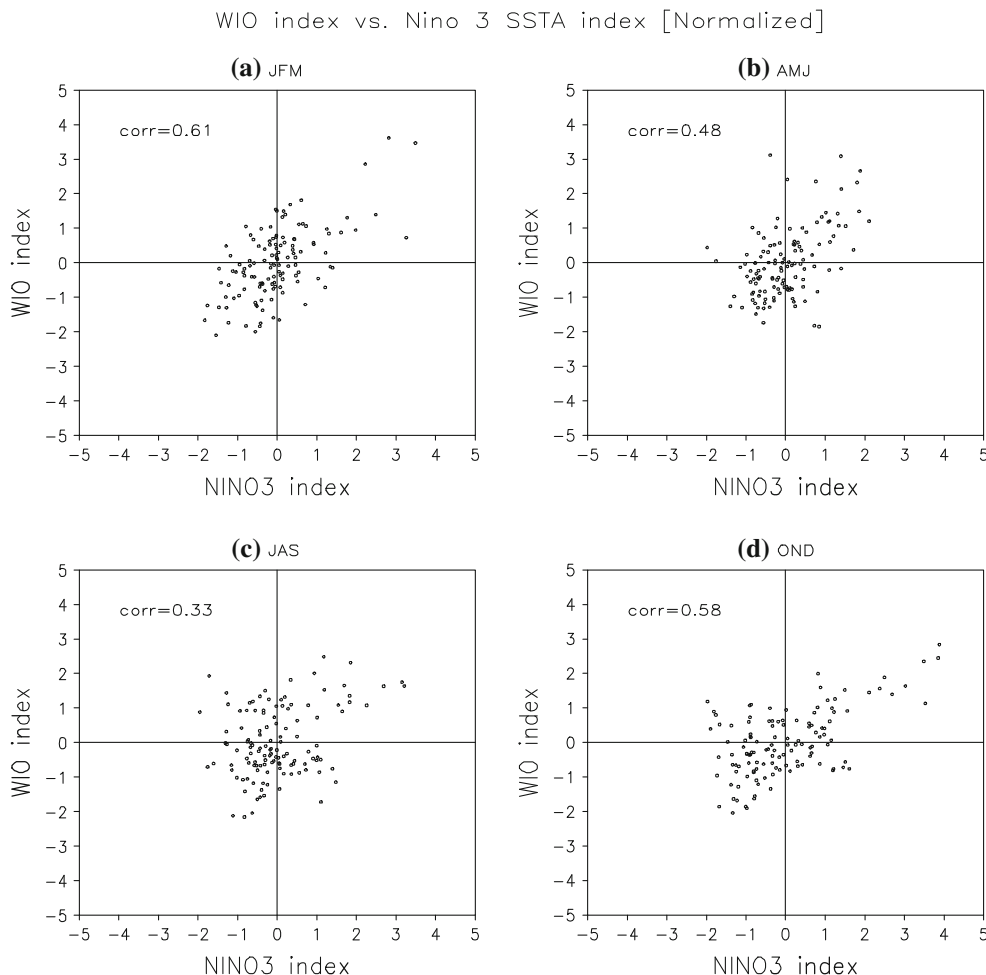


Fig. 4 Scatter plot and correlation between Nino 3 SSTA index and the western component of IOD index (WIO; 50°E – 70°E , 10°S – 10°N), normalized by their standard deviation, for **a** JFM, **b** AMJ, **c** JAS, and

d OND. Nino3 SSTA and WIO indices are calculated using ERA-40 reanalysis monthly data from 1959 to 1999

El Nino during the winter of 1987 affect the IOD? How does the similar forcing affect the IOD in other seasons?

The scatter plot between IOD index and Nino3 index for different seasons is constructed using SST of ERA-40 reanalysis data from 1959 to 1999 (Fig. 2). Statistical significance of the correlation coefficients is determined by a two-tailed “*t* test”. The results indicate that the occurrence of El Nino from January until June does not necessarily favor the development of IOD. For example, the correlation between Nino3 index and IOD index in JFM is negative (Fig. 2a, $r = -0.22$) and insignificant (below 90% significance level). The correlation between Nino3 and IOD becomes significantly positive (above 99% significance level) only during JAS (Fig. 2c, $r = 0.44$) and OND (Fig. 2d, $r = 0.56$). This is similar to the results when a significant correlation of 0.52 is obtained between mean SON values of the Saji et al. (1999) IOD index and Nino3, using data from 1872 to 1997. The correlation using only

the shorter post-1957 period examined by Saji et al. (1999) is 0.56 (Allan et al. 2001). It implies that the relationship between El Nino and IOD varies throughout the seasons. This seasonality becomes more obvious when correlation in SST between Nino3 region and eastern part of the IOD (EIO, 90–110°E, 10°S-equator) is calculated (Fig. 3). The positive (negative) correlation between Nino3 index and EIO index in JFM and AMJ (JAS and OND) indicates that the cooling of eastern Indian Ocean, in association with the El Nino forcing, is active only during the latter period. More importantly, the development of El Nino during JFM and AMJ, accompanies the warming of eastern Indian Ocean. The correlations for JFM ($r = 0.64$) and AMJ ($r = 0.35$) are significant at the 99 and 95% levels respectively, while for JAS ($r = -0.22$) and OND ($r = -0.17$) the significance drops below 90% levels. Considering that the correlation between Nino3 and western part (WIO; 50–70°E, 10°S–10°N) of IOD is always significantly positive (at 99%

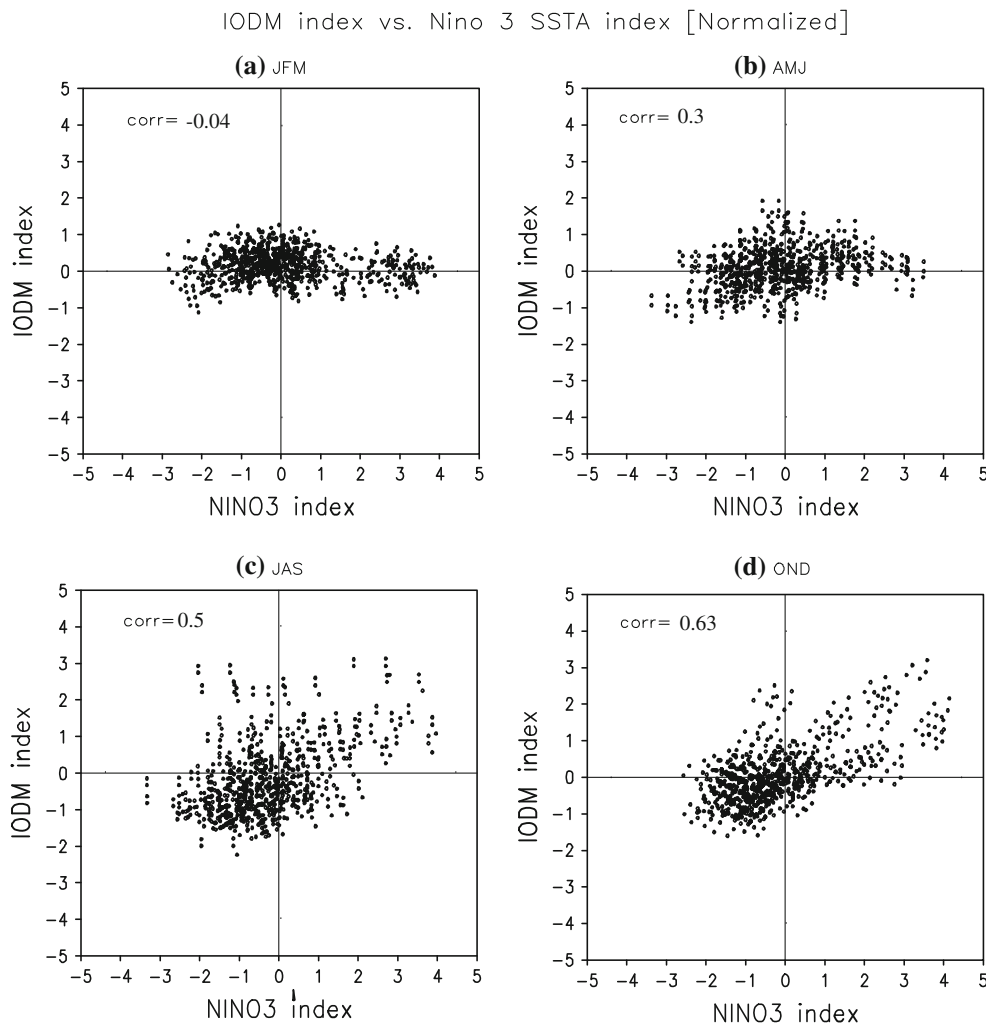


Fig. 5 Scatter plot and correlation between Nino3 SST index and IOD indices, normalized by their standard deviation, obtained from the twentieth century run (20c3m; 1861–2000) by GFDL_CM2.1 model.

For each season of **a** JFM, **b** AMJ, **c** JAS, and **d** OND, five parallel runs of 140 year simulation are used (5 runs \times 140 years = 700)

significance levels for all seasons, except for JAS where it is 95%) throughout the seasons (Fig. 4), the seasonality of El Nino forcing on the Indian Ocean appears to be more sensitive in the eastern part (EIO) of the dipole. The objective of this study is to understand why the occurrence/existence of El Nino during JFM and AMJ is not favorable for the IOD, especially in the eastern part of Indian Ocean.

The scatter plot between IOD index and Nino3 index for different seasons is constructed using SST of CM2.1 (Fig. 2). Consistent with the observations, the correlation between Nino3 index and IOD index in JFM is negative (Fig. 5a, $r = -0.04$) and becomes significantly positive (above 99% significance level) only during JAS (Fig. 5c, $r = 0.5$) and OND (Fig. 5d, $r = 0.63$). Scatter plots of Nino3 and EIO for different seasons in CM2.1 are shown in Fig. 6. Similar to the observations (Fig. 3), the positive correlation (at 99% significance levels) between Nino3 and EIO is found in JFM (Fig. 6a, $r = 0.74$) and AMJ (Fig. 6b, $r = 0.62$). It implies that when El Nino becomes stronger in these months, the SST in the eastern Indian Ocean increases.

This positive relationship is no longer held in JAS (Fig. 6c, $r = -0.15$) and OND (Fig. 6d, $r = -0.06$), when the strengthening of El Nino is associated with the cooling of the eastern Indian Ocean. Also, in agreement with the ERA-40 results (Fig. 4), the seasonal modulation of the correlation is less obvious in the western part of the IOD (WIO; Fig. 7). Although there is a seasonal variation in the magnitude of the correlation, the positive correlation between Nino3 and WIO persists throughout the year. These results indicate that CM2.1 can simulate the observed seasonality between El Nino and IOD, reasonably well. In the next section, the spatial structure of atmospheric and oceanic variables, associated with the El Nino is examined in detail.

4 Spatial structure of seasonal variation associated with the El Nino in GFDL_CM_2.1

The atmospheric circulation associated with El Nino may result in various impacts on the Indian Ocean, depending

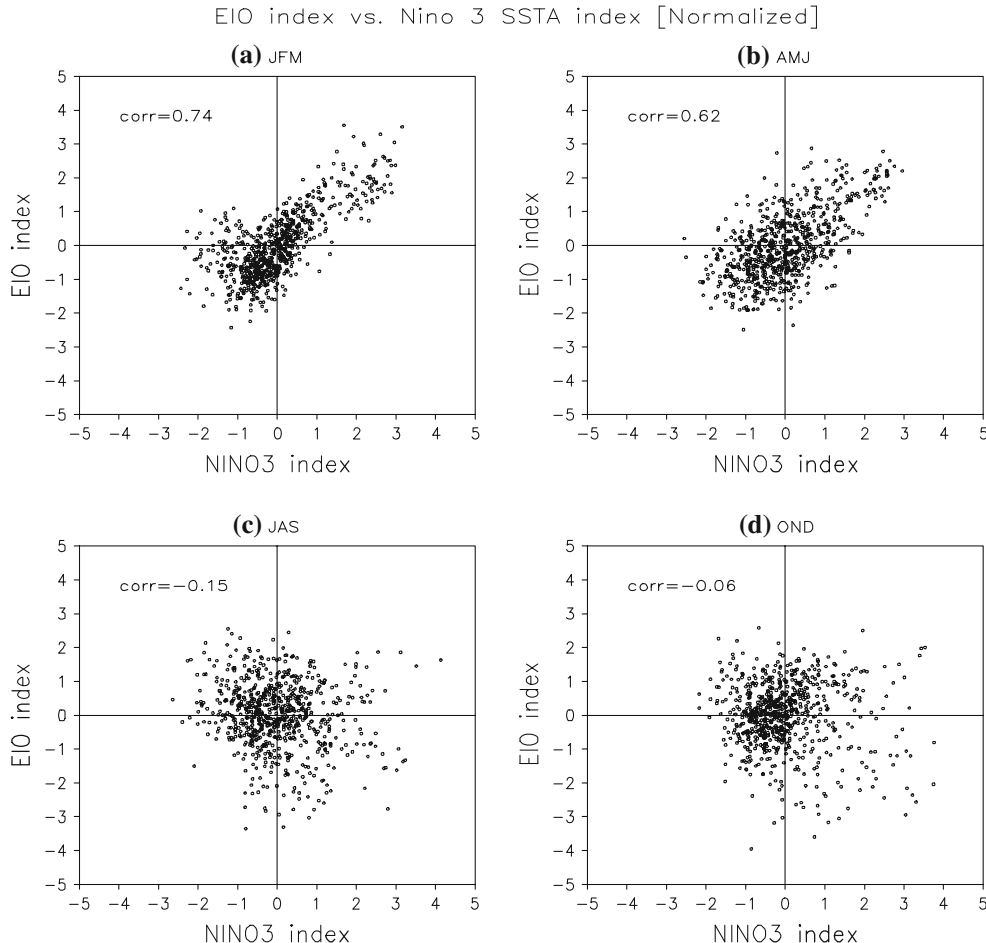


Fig. 6 Scatter plot and correlation between Nino3 SSTA index and the eastern component of IOD index (EIO; 90–110E, 10S-Equator), normalized by their standard deviation, obtained from the twentieth

century run (20c3m; 1861–2000) by GFDL_CM2.1 model. For each season of **a** JFM, **b** AMJ, **c** JAS, and **d** OND, five parallel runs of 140 year simulation are used ($5 \text{ runs} \times 140 \text{ years} = 700$)

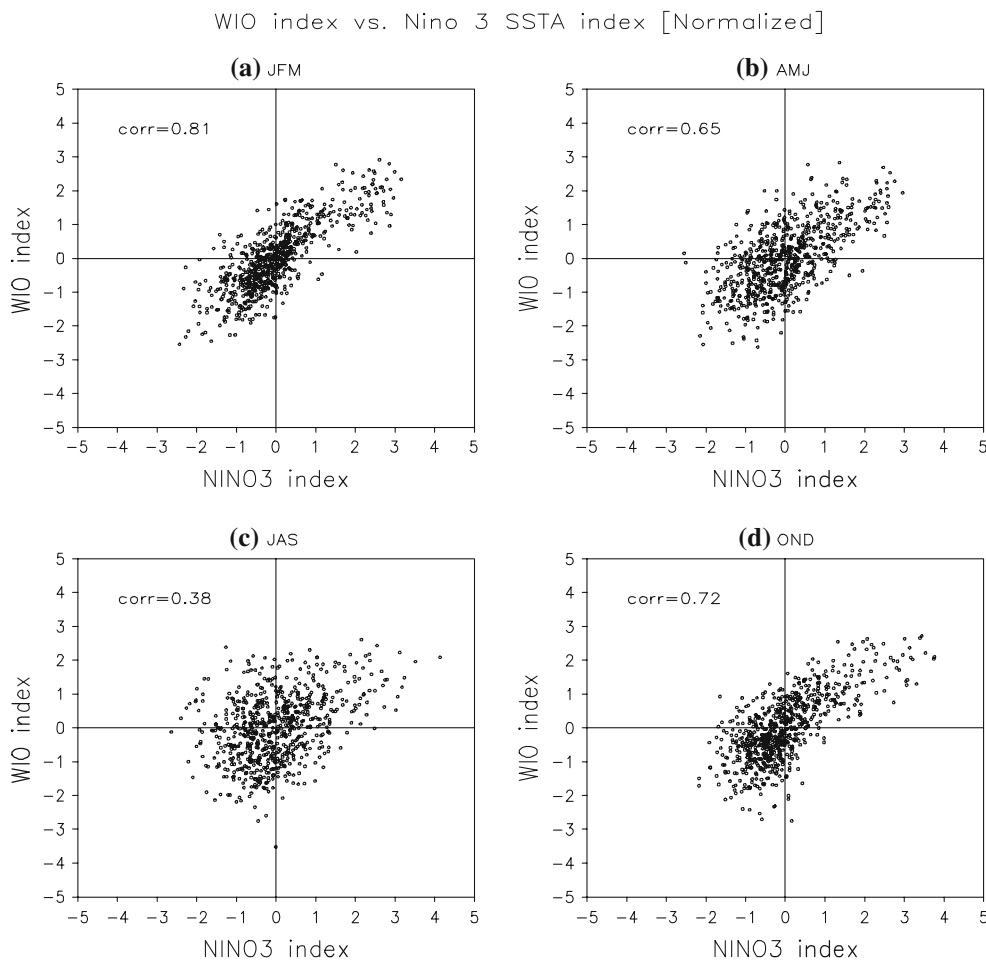


Fig. 7 Scatter plot and correlation between Nino3 SSTA index and the eastern component of IOD index (EIO; 90–110E, 10S-Equator), normalized by their standard deviation, obtained from the twentieth

century run (20c3m; 1861–2000) by GFDL_CM2.1 model. For each season of **a** JFM, **b** AMJ, **c** JAS, and **d** OND, five parallel runs of 140 year simulation are used (5 runs \times 140 years = 700)

on the phase of the seasonal cycle. The phase locking between El Nino forcing and seasonal mean circulation over the Indian Ocean has already been addressed in several studies. For example, the importance of the wind anomalies over the Indian Ocean in boreal spring/early summer is studied by Annamalai et al. (2003). They suggested that when ENSO-like conditions exist in the western Pacific, the coupled variability of the eastern equatorial Indian Ocean intensifies in boreal spring/early summer. They called the boreal spring/summer a “time window”, since in this period the ocean–atmosphere system is particularly sensitive to external forcing. It is also shown in the study by Zhong et al. (2005) that if the El Nino event develops later than boreal summer, it is incapable of inducing strong dynamic coupling in the Indian Ocean and fails to produce the IOD mode. The merit of this study is to identify and investigate the mechanisms through which the anomalies induced by El Nino on the eastern Indian Ocean

may have negative consequences on the development of IOD episodes, depending on their phase relative to the seasonal cycle. Thus, our focus is to understand why the existence of El Nino anomalies during JFM is unfavorable for the IOD in the following autumn, while the similar forcing in later seasons (e.g. spring–summer) facilitates the development of IOD.

4.1 Spatial structure in JFM

For the seasonal mean of the correlation map, the monthly data of the 20c3m (1861–2000) simulation from five parallel members (140 years \times 5 members) by CM2.1 are seasonally averaged for JFM, AMJ, JAS, and OND. Then the seasonal mean anomalies are correlated with the seasonal mean Nino3 index.

In JFM, the warming of SST is detected from the equatorial Indian Ocean to the eastern Pacific Ocean

(Fig. 8a). The sea level pressure (SLP) decreases over the equatorial eastern Pacific Ocean (Fig. 8b), where the maximum increase of SST is located (Fig. 8a). Over the region between the western Indian Ocean and the western Pacific Ocean, the SLP increases with the maximum over the maritime continent. Associated with this maximum increase of the SLP at the maritime continent, an anti-cyclonic circulation develops in the southeastern Indian Ocean between off the coast of Sumatra and northwestern Australia (Fig. 8b). At the same time, the climatology of SLP at the maritime continent is dominated by a local minimum, accompanying by a climatological cyclonic circulation over the region (Fig. 8c).

This increase in the anti-cyclonic circulation in the anomalous winds (Fig. 8b) counteract on the cyclonic circulation of climatological wind field (Fig. 8c). This results in reduced mean winds, which causes reduced upward latent heat flux anomalies (Fig. 8d) over the EIO. The latent heat flux contributes to the net surface heat flux, along with sensitive heat, shortwave radiation and long

wave radiation fluxes. In the tropical regions, the latent heat flux tends to dominate surface heat flux variability (Q), and a positive feedback takes place between the wind-induced flux and SST (Behera et al. 2000). Thus, the reduced upward latent heat flux anomalies in this region contribute to the enhancement of downward net surface flux anomalies (Q' ; Fig. 8e) and in turn, extend the positive SST anomalies from the equator up to the EIO. These results imply that the JFM forcing of the IOD tends to be opposite to that of the forcing later in the year (e.g. JAS), when a positive IOD is on average forced.

The enhancement of anti-cyclonic wind stress (Fig. 8b) may also induce open ocean Ekman downwelling. This is observed from the downward vertical motion averaged for the upper 100 m of ocean, which increases in the region south of the equator, extending up to the western coast of Australia (Fig. 8f). Such a downwelling will assist the warming of the EIO, apart from that due to the net surface flux anomalies. In summary, the El Niño induced anti-cyclonic anomalous circulation over the southeastern

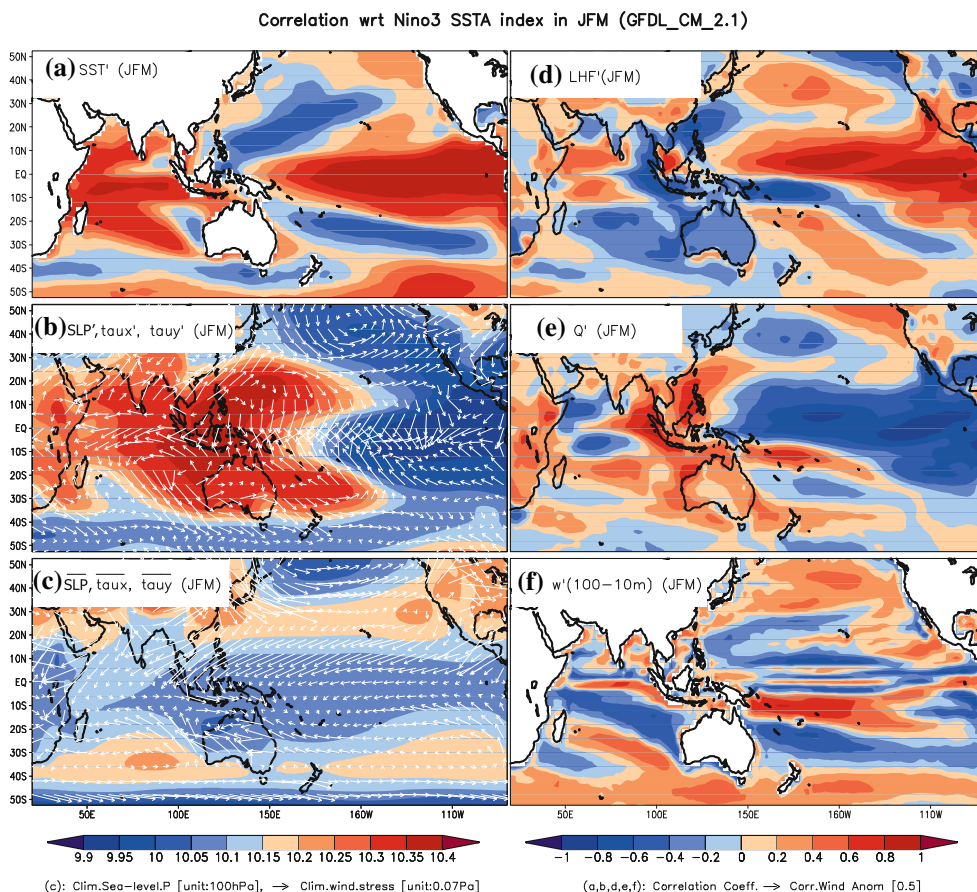


Fig. 8 Maps of correlation between JFM mean anomalies of **a** SST, **b** sea level pressure and wind stress, **d** latent heat flux, **e** surface net heat flux, and **f** vertical motion averaged within upper 100 m of ocean; and JFM mean Nino 3 SST anomalies. **c** Climatology of JFM

mean sea level pressure and wind stress. The color bar and wind legend in the right side represent the correlation coefficient of **a**, **b**, **d**, **e**, and **f** panels. The color bar [100 hPa] and wind legend [0.07 Pa] in the left side applies to **c** panel

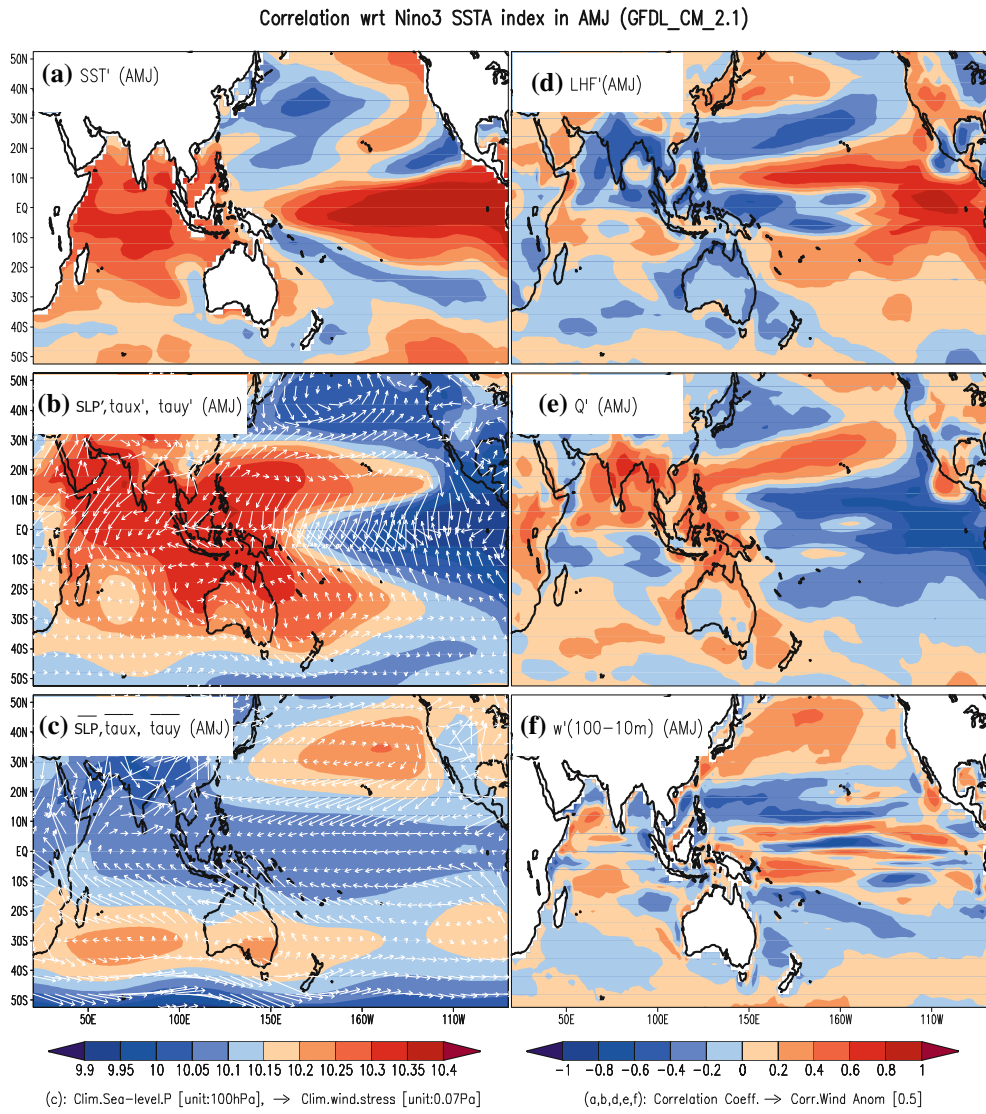


Fig. 9 Same as Fig. 8, except for the AMJ mean

Indian Ocean in JFM accounts for the warming of the southeastern Indian Ocean, a condition unfavorable (favorable) for the development of a positive (negative) IOD.

4.2 Spatial structure in AMJ

The presence of El Niño in JFM (Sect. 4.1) tends to suppress the development of positive IOD by inducing positive downward net surface flux anomalies, a condition that resembles the reversed phase of IOD (Fig. 8e). During AMJ, however, the interaction between anomalous and climatological winds no longer induces the reversed phase of IOD in the downward net surface flux anomalies (Fig. 9e). This is because, the anomalous anti-cyclonic circulation (Fig. 9b) and the climatological southeasterlies

(Fig. 9c) over the southeastern Indian Ocean produce a region between 80–100°E and 15–5°S, where both anomalies and climatological winds are easterlies. Over the northwestern Indian Ocean, on the other hand, the anomalous winds (Fig. 9b) are in opposite direction to the climatological monsoon flows (Fig. 9c). This results in the decrease (increase) of the downward net surface flux in the southeastern Indian Ocean (northwestern Indian Ocean). Thus, the spatial structure of the net surface flux anomalies during AMJ rather resembles a transition towards the positive phase of IOD (Fig. 9e).

4.3 Spatial structure in JAS

The development of IOD in association with the El Niño becomes apparent in JAS (Fig. 10a). The warming of the

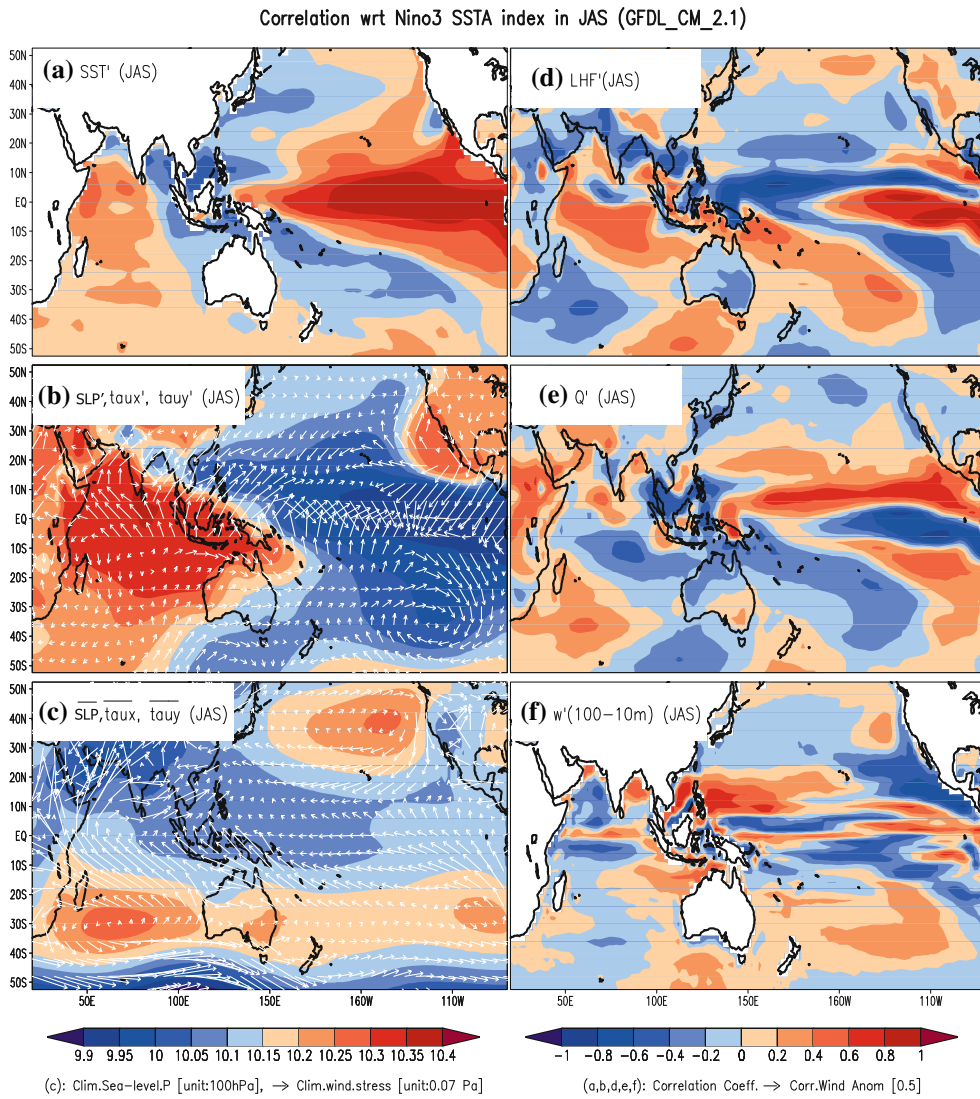


Fig. 10 Same as Fig. 8, except for the JAS mean

western part of IOD ($50\text{--}70^{\circ}\text{E}$, $10^{\circ}\text{S}\text{--}10^{\circ}\text{N}$) and the cooling of the eastern part of IOD ($90\text{--}100^{\circ}\text{E}$, 10°S -equator) progress with the increasing SST anomalies in the eastern Pacific Ocean. The enhanced upward latent heat flux anomalies (Fig. 10d), resulting in the reduced downward net surface flux anomalies (Fig. 10e) in the western and central Indian Ocean, play a negative feedback by damping out the increased SST anomalies in these regions (Fig. 10a). In contrast, the downward (upward) motion in the upper 100 m of western (southeastern) Indian Ocean further amplifies the warming (cooling) of the western (southeastern) Indian Ocean (Fig. 10f). This positive feedback from the oceanic component in JAS is known to be crucial for the further development of IOD in OND (e.g. Annamalai et al. 2003; Gualdi et al. 2003; Lau and Nath 2003; Li et al. 2003; Loschnigg et al. 2003; Shinoda et al. 2004a; Cai et al. 2005).

4.4 Spatial structure in OND

The positive phase of IOD reaches its maximum in OND (Fig. 11a). During this period, the seasonal shift of the climatological winds (Fig. 11c) occurs, and the interaction between anomalous and climatological winds suppresses further intensification of IOD in following seasons. That is, the anomalous anti-cyclonic circulation in the southeastern Indian Ocean (Fig. 11b) is no longer in phase with the climatological wind stress (Fig. 11c).

Consequently, the reduction (enhancement) of the upward latent heat flux (downward net surface flux) is evident from the southeastern Indian Ocean to the Australia (Fig. 11e). Comparison between net heat flux anomalies among JFM (Fig. 8e), AMJ (Fig. 9e), and OND (Fig. 11e) implies that even if a similar anomalous anti-cyclonic circulation presides over the southeastern Indian Ocean, it

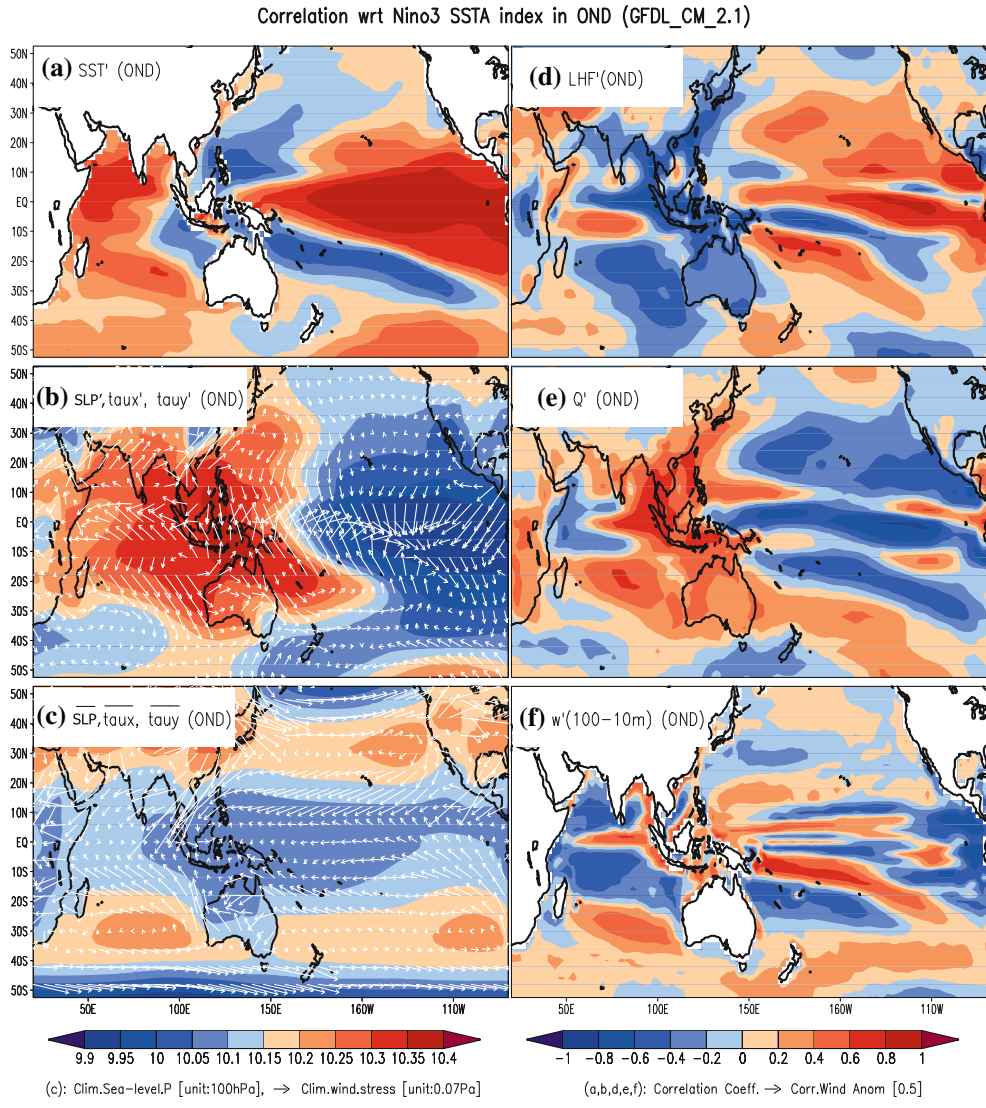


Fig. 11 Same as Fig. 8, except for the OND mean

can either increase or decrease the net heat flux anomalies, depending on its phase locking with climatological winds.

5 Summary and discussion

In this study, the seasonality in the relationship between El Nino and IOD is examined in order to explain why there are El Nino episodes that, though weak, appear to act as triggers to IOD events; whereas other El Ninos, though much stronger, do not initiate any IOD. The correlation in SST between the eastern part of Indian Ocean (EIO) and the eastern Pacific Ocean (Niño3) are positive during January-March (JFM) and last until April-June (AMJ). This positive correlation in the first half of the year reverses from July through December due to the evolution of the

seasonal cycle in the Indian Ocean. Since there is little seasonal change in the relationship between Niño3 and western part of the Indian Ocean dipole (WIO), the main cause of the seasonality in the correlation between El Nino and IOD is from the eastern part of the Indian Ocean. That is, a development of El Nino during JFM of YEAR0 (JAS of YEAR0) is unfavorable (favorable) for the development of IOD, since it accompanies the warming (cooling) of the southeastern Indian Ocean. The analysis of the spatial structure of atmospheric and oceanic variables reveals that when El Nino develops early in the preceding winter season (JFM of YEAR0), the anomalous anti-cyclonic circulation over the southeastern Indian Ocean clashes with the climatological winds, resulting in the reduction of upward latent heat flux anomalies, and the increase of the net downward surface heat flux anomalies. This atmospheric response in the winter season appears to be the reason for

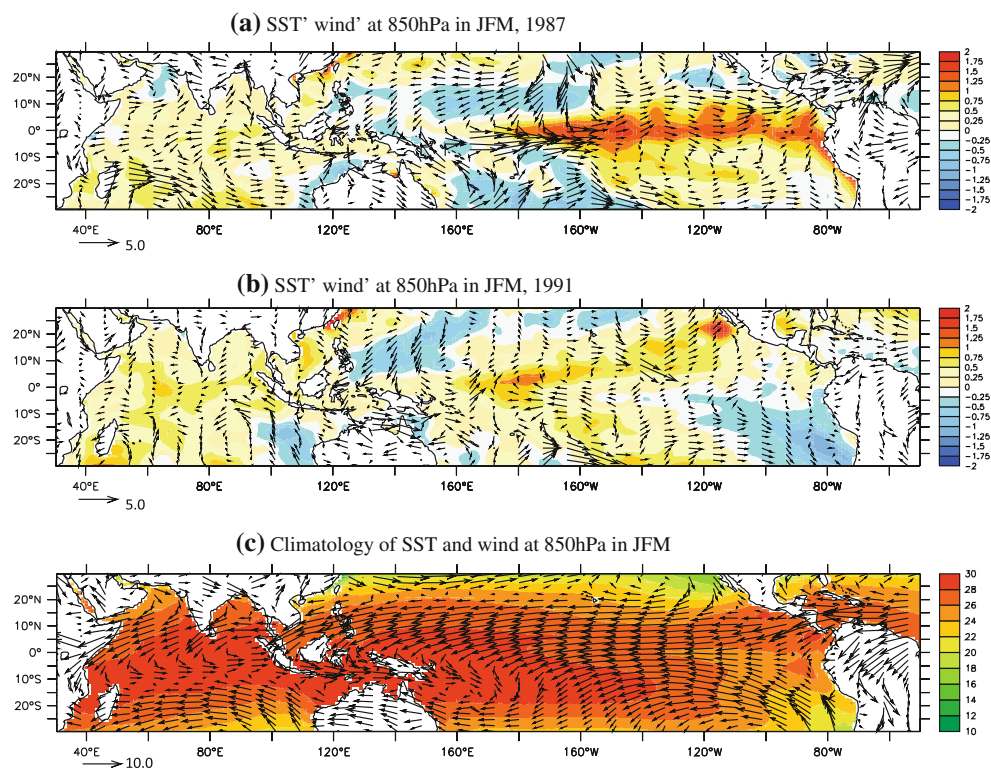
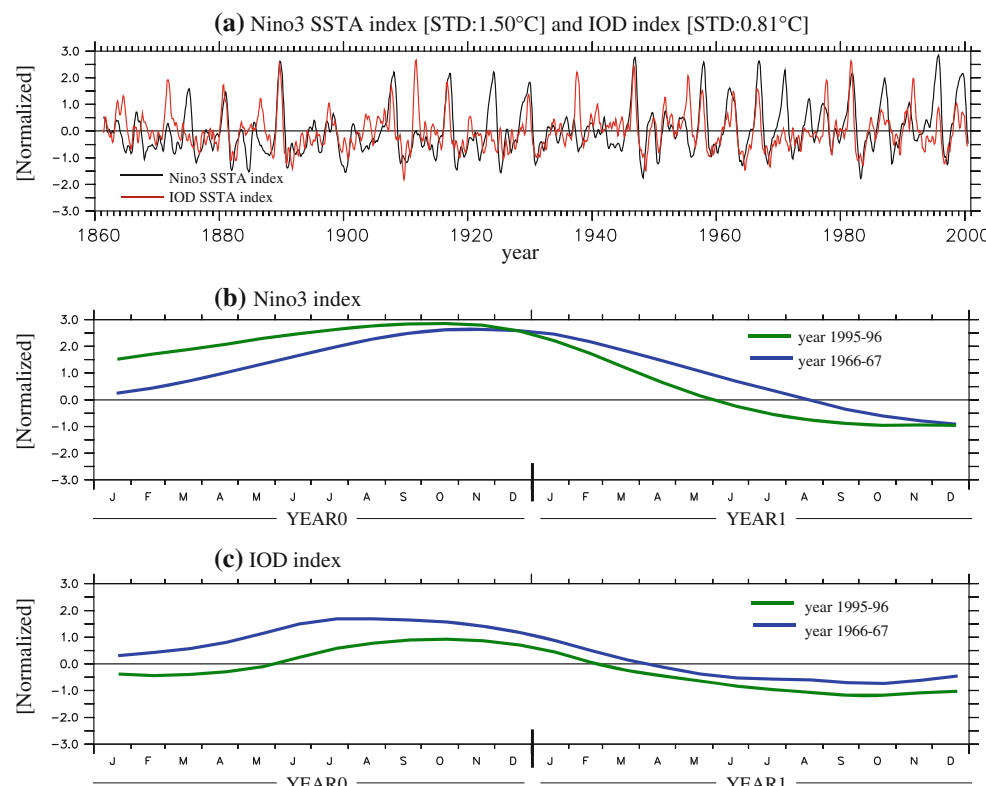


Fig. 12 JFM mean of SST (colors; °C) and wind anomalies (arrows, m s^{-1}) at 850 hPa in **a** 1987 and **b** 1991. **c** Climatology of JFM mean SST (colors; °C) and wind (arrows, m s^{-1}) at 850 hPa. The ERA-40 reanalysis data, from 1959 to 1999 is used

Fig. 13 **a** Nino 3 and IOD SSTA indices normalized by their standard deviation, for the period 1861–2000, estimated from the twentieth century run (20c3m; 1861–2000) by GFDL_CM2.1 model. Normalized **b** Nino3 and **c** IOD SSTA indices for the years 1995–1996 and 1966–1967. The climatology from 1861 to 2000 is used to calculate the anomalous monthly SST. Then, 8-month running mean is applied to these anomalies in order to highlight the interannual variability



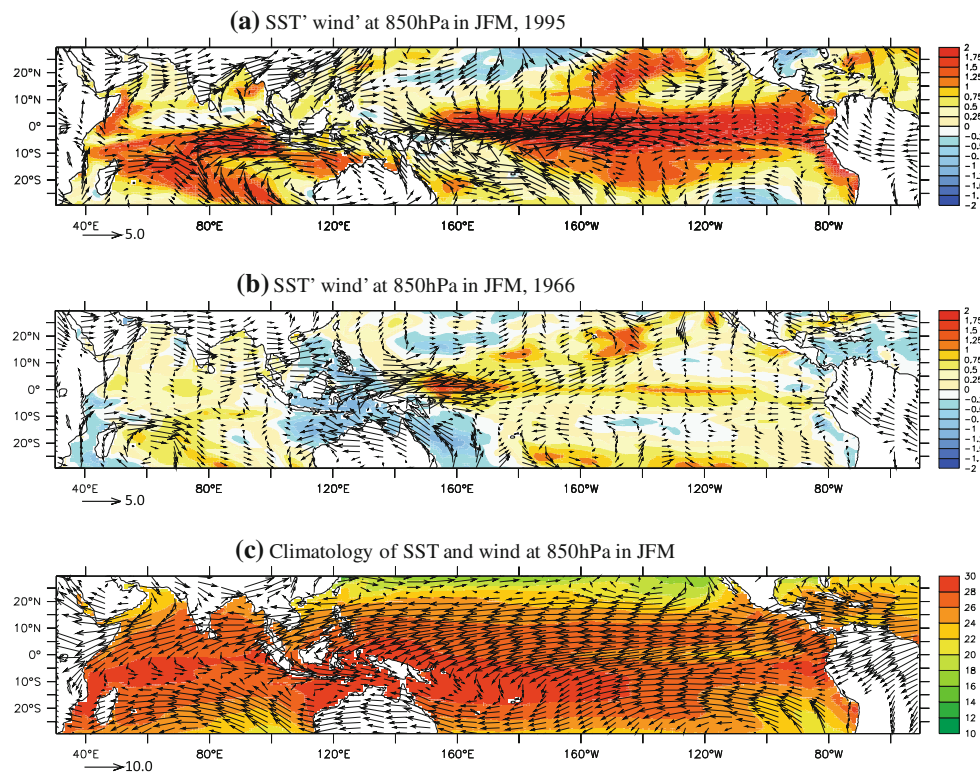


Fig. 14 JFM mean of SST (colors; °C) and wind anomalies (arrows, m s^{-1}) at 850 hPa in **a** 1995 and **b** 1966, from the twentieth century run (20c3m; 1861–2000) by GFDL_CM2.1 model. **c** Climatology of JFM mean SST (colors; °C) and wind (arrows, m s^{-1}) at 850 hPa

the warming of the eastern Indian Ocean observed in winter of El Nino years. It is widely accepted that a strong El Nino can trigger the development of an IOD. The implication of our study is that when El Nino is in moderate magnitude, such as the one in the year 1987 or 1991 (in ERA-40), the phase locking between El Nino and seasonal cycle over the Indian Ocean could be an important factor that affects the development of the IOD. For example, the presence of the El Nino during JFM of the year 1987 induces the anti-cyclonic anomalies over the southeastern Indian Ocean (Fig. 12a). These anomalous winds are opposite to the climatological winds (Fig. 12c). Placing these results along with the monthly variability of the Nino3 and IOD indices (Fig. 1b) confirms that the early appearance of the El Nino forcing during the winter (JFM) of 1987 is not favorable for the development of IOD (Fig. 1c). Meanwhile for the year 1991, without an early development of El Nino during the winter, the anomalous winds are less counteracting to the climatological winds (Fig. 12b). This infers why the IOD in 1987 is weaker than that of 1991, even though the El Nino in 1987 is stronger than that in 1991 (Fig. 1).

Investigation of El Nino events in the CM2.1 also gives similar results for El Nino years. Figure 13a shows the interannual variability of the Nino3 and IOD indices. Most of the El Nino events occur along with an IOD event.

However, it is to be noted that there are a few events with the Nino3 index being above 1.0 standard deviation and the IOD index remarkably weak. Out of these El Nino years, 2 distinct years were selected for examining the early development of El Nino in the winter (years 1966–1967) and later development of El Nino in spring-summer (years 1995–1996). During 1995, the presence of El Nino anomalies is seen from JFM (Fig. 13b) and as a result, the IOD is weak during this year (Fig. 13c). As in ERA-40, the presence of the El Nino anomalies during the preceding winter induces anti-cyclonic anomalies over the southeastern Indian Ocean (Fig. 14a). These anomalous winds counteract the climatological winds (Fig. 14c) which induces increased downward net surface flux anomalies, increasing the SST over the southeastern Indian Ocean. Meanwhile during 1966, the El Nino anomalies are absent in the winter and develops only late in spring-summer (Fig. 13c) and this is accompanied by strong IOD events in the same year. This is due to the anomalous winds which are less counteracting to the climatological winds (Fig. 14b) and hence, favorable for the development of an IOD. Thus, the findings from this study suggest that anti-cyclonic circulation anomalies over the southeastern Indian Ocean during JFM accounts for the warming of the southeastern Indian Ocean and a weakened IOD structure. Meanwhile, development of the El Nino anomalies late in

spring-summer results in much weaker anti-cyclonic circulation anomalies and hence, enhancement of a positive phase of an IOD.

Consistent with the previous studies (Wittenberg et al. 2006; Song et al. 2007a), the model reproduces the fundamental characteristics of the interannual SST variability of the Pacific and Indian Oceans, the occurrence of El Niño and IOD events, and the statistical relationship between El Niño and IOD. CM2.1 is also found to simulate the observed seasonality between El Niño and IOD, reasonably well. However, CM2.1 has shortcomings common to many GCMs; for example the mean SST along the equatorial Pacific is 1–2°C too cold, the mean trade winds, deep convection and tropical precipitation anomalies are shifted westward. Also, there are unrealistic features in the Indian ocean, including cooler mean SST, stronger surface winds, and more equatorially confined precipitation (Song et al. 2007b). These factors might affect the results in the present study, and are to be taken into account while considering the El Niño–IOD relationship in the model.

It is found that downward vertical motion has a role in some cases (e.g. JFM, Fig. 8f) in assisting the warming of the EIO, other than the active role by the net surface flux anomalies. This brings into light the importance of investigating the potential role played by ocean dynamics viz. the Indonesian throughflow (ITF), in getting a better perspective of the IOD–El Niño interactions (Bracco et al. 2005; England and Huang 2005; Song et al. 2007b). However, a detailed analysis of the role of the ITF is beyond the aim of this paper and deserves a specific and more in depth investigation.

Acknowledgments The authors thank the international modeling group and the program for climate model diagnostic and inter-comparison for providing the data. This work has been supported by the Italy-US cooperation Program in Climate Science and Technology by the European Community project ENSEMBLE, contract GOCE-CT-2003-505539. First author is thankful to the Centre for Climate Change Research at the Indian Institute of Tropical Meteorology for facilitating part of the review process. Constructive suggestions and comments from two anonymous reviewers have helped in improving this paper.

References

- Allan R, Chambers D, Drosdowsky W, Hendon HH, Latif M, Nicholls N, Smith I, Stone RC, Tourre Y (2001) Is there an Indian Ocean dipole and is it independent of the El Niño–Southern Oscillation? CLIVAR Exch 6:18–22
- Anderson JL, Balaji V, Broccoli AJ, Cooke WF, Delworth TL, Dixon KW, Donner LJ, Dunne KA, Freidenreich SM, Garner ST, Gudgel RG, Gordon CT, Held IM, Hemler RS, Horowitz LW, Klein SA, Knutson TR, Kushner PJ, Langenhorst AR, Lau NC, Liang Z, Malyshev SL, Milly PCD, Nath MJ, Ploshay JJ, Ramaswamy V, Schwarzkopf MD, Shevliakova E, Sirutis JJ, Soden BJ, Stern WF, Thompson LA, Wilson RJ, Wittenberg AT, Wyman BL, Dev GGAM (2004) The new GFDL global atmosphere and land model AM2-LM2: evaluation with prescribed SST simulations. *J Clim* 17:4641–4673
- Annamalai H, Murtugudde R, Potemra J, Xie SP, Liu P, Wang B (2003) Coupled dynamics over the Indian Ocean: spring initiation of the Zonal Mode. *Deep Sea Res Part 2 Top Stud Oceanogr* 50:2305–2330
- Ashok K, Guan ZY, Saji NH, Yamagata T (2004) Individual and combined influences of ENSO and the Indian Ocean Dipole on the Indian summer monsoon. *J Clim* 17:3141–3155
- Behera SK, Salvekar PS, Yamagata T (2000) Simulation of interannual SST variability in the tropical Indian Ocean. *J Clim* 13:3487–3499
- Behera SK, Luo JJ, Masson S, Delecluse P, Gualdi S, Navarra A, Yamagata T (2005) Paramount impact of the Indian Ocean dipole on the East African short rains: a CGCM study. *J Clim* 18:4514–4530
- Black E, Slingo J, Sperber KR (2003) An observational study of the relationship between excessively strong short rains in coastal East Africa and Indian Ocean SST. *Mon Weather Rev* 131:74–94
- Bracco A, Kucharski F, Molteni F, Hazeleger W, Severijns C (2005) Internal and forced modes of variability in the Indian Ocean. *Geophys Res Lett* 32:L12707
- Cai WJ, Hendon HH, Meyers G (2005) Indian Ocean dipole-like variability in the CSIRO mark 3 coupled climate model. *J Clim* 18:1449–1468
- Delworth TL, Broccoli AJ, Rosati A, Stouffer RJ, Balaji V, Beesley JA, Cooke WF, Dixon KW, Dunne J, Dunne KA, Durachta JW, Findell KL, Ginoux P, Gnanadesikan A, Gordon CT, Griffies SM, Gudgel R, Harrison MJ, Held IM, Hemler RS, Horowitz LW, Klein SA, Knutson TR, Kushner PJ, Langenhorst AR, Lee HC, Lin SJ, Lu J, Malyshev SL, Milly PCD, Ramaswamy V, Russell J, Schwarzkopf MD, Shevliakova E, Sirutis JJ, Spelman MJ, Stern WF, Winton M, Wittenberg AT, Wyman B, Zeng F, Zhang R (2006) GFDL's CM2 global coupled climate models. Part I: formulation and simulation characteristics. *J Clim* 19:643–674
- Drbohlav HKL, Gualdi S, Navarra A (2007) A diagnostic study of the Indian Ocean dipole mode in El Niño and non-El Niño years. *J Clim* 20:2961–2977
- England MH, Huang F (2005) On the interannual variability of the Indonesian throughflow and its linkage with ENSO. *J Clim* 18:1435–1444
- Fischer AS, Terray P, Guilyardi E, Gualdi S, Delecluse P (2005) Two independent triggers for the Indian Ocean dipole/zonal mode in a coupled GCM. *J Clim* 18:3428–3449
- Griffies SM, Harrison MJ, Pacanowski RC, Rosati A (2003) A technical guide to MOM4. NOAA/GFDL, Princeton, NJ
- Gualdi S, Guilyardi E, Navarra A, Masina S, Delecluse P (2003) The interannual variability in the tropical Indian Ocean as simulated by a CGCM. *Clim Dyn* 20:567–582
- Iizuka S, Matsuura T, Yamagata T (2000) The Indian Ocean SST dipole simulated in a coupled general circulation model. *Geophys Res Lett* 27:3369–3372
- Lau NC, Nath MJ (2003) Atmosphere–ocean variations in the Indo-Pacific sector during ENSO episodes. *J Clim* 16:3–20
- Li T, Wang B, Chang CP, Zhang YS (2003) A theory for the Indian Ocean dipole-zonal mode. *J Atmos Sci* 60:2119–2135
- Loschnigg J, Meehl GA, Webster PJ, Arblaster JM, Compo GP (2003) The Asian monsoon, the tropospheric biennial oscillation, and the Indian Ocean zonal mode in the NCAR CSM. *J Clim* 16:1617–1642
- Saji NH, Yamagata T (2003a) Possible impacts of Indian Ocean Dipole mode events on global climate. *Clim Res* 25:151–169
- Saji NH, Yamagata T (2003b) Structure of SST and surface wind variability during Indian Ocean dipole mode events: COADS observations. *J Clim* 16:2735–2751

- Saji NH, Goswami BN, Vinayachandran PN, Yamagata T (1999) A dipole mode in the tropical Indian Ocean. *Nature* 401:360–363
- Shinoda T, Alexander MA, Hendon HH (2004a) Remote response of the Indian Ocean to interannual SST variations in the tropical Pacific. *J Clim* 17:362–372
- Shinoda T, Hendon HH, Alexander MA (2004b) Surface and subsurface dipole variability in the Indian Ocean and its relation with ENSO. *Deep Sea Res Part I Oceanogr Res Pap* 51:619–635
- Song Q, Vecchi GA, Rosati AJ (2007a) Indian Ocean variability in the GFDL coupled climate model. *J Clim* 20:2895–2916
- Song Q, Vecchi GA, Rosati AJ (2007b) The role of the Indonesian throughflow in the Indo-Pacific climate variability in the GFDL coupled climate model. *J Clim* 20:2434–2451
- Terray P, Delecluse P, Labattu S, Terray L (2003) Sea surface temperature associations with the late Indian summer monsoon. *Clim Dyn* 21:593–618
- Webster PJ, Moore AM, Loschnigg JP, Leben RR (1999) Coupled ocean-atmosphere dynamics in the Indian Ocean during 1997–98. *Nature* 401:356–360
- Wittenberg AT, Rosati A, Lau NC, Poshay JJ (2006) GFDL's CM2 global coupled climate models. Part III: tropical pacific climate and ENSO. *J Clim* 19:698–722
- Yamagata T, Behera S, Rao SA, Guan Z, Ashok K, Saji NH (2002) The Indian Ocean dipole: a physical entity. CLIVAR Exchanges, vol 24. International CLIVAR Project Office, Southampton, United Kingdom, pp 15–18, 20–22
- Yuan Y, Li CY (2008) Decadal variability of the IOD-ENSO relationship. *Chin Sci Bull* 53:1745–1752
- Zhong AH, Hendon HH, Alves O (2005) Indian Ocean variability and its association with ENSO in a global coupled model. *J Clim* 18:3634–3649